

1
2
3
4
5
6
7
8
9
10
11
12
13
14
15
16
17
18
19
20
21
22
23
24
25
26
27
28
29
30
31
32
33
34
35
36
37
38

Dietary pectic glycans are degraded by coordinated enzyme pathways in human colonic *Bacteroides*

Ana S. Luis^{1¶}, Jonathon Briggs^{1¶}, Xiaoyang Zhang^{1¶}, Benjamin Farnell^{2,3}, Didier Ndeh¹, Aurore Labourel¹, Arnaud Baslé¹, Alan Cartmell¹, Nicolas Terrapon⁴, Katherine Stott⁵, Elisabeth C. Lowe¹, Richard McLean², Kaitlyn Shearer², Julia Schückerl⁶, Immacolata Venditto¹, Marie-Christine Ralet⁷, Bernard Henrissat^{4,8,9}, Eric C. Martens¹⁰, Steven C. Mosimann³, D. Wade Abbott^{2,3*} and Harry J. Gilbert^{1,*}

¹*Institute for Cell and Molecular Biosciences, Newcastle University, Newcastle upon Tyne NE2 4HH, U.K.*

²*Lethbridge Research and Development Centre, Agriculture and Agri-Food Canada, Lethbridge, Alberta, Canada, T1J 4B1*

³*Department of Chemistry and Biochemistry, University of Lethbridge, Lethbridge, Alberta, Canada, T1K 6T5*

⁴*Architecture et Fonction des Macromolécules Biologiques, Centre National de la Recherche Scientifique (CNRS), Aix-Marseille University, F-13288 Marseille, France*

⁵*Department of Biochemistry, University of Cambridge, Cambridge, United Kingdom*

⁶*Department of Plant and Environmental Sciences, Faculty of Science, University of Copenhagen, Copenhagen, Denmark*

⁷*INRA, UR1268 Biopolymères Interactions Assemblages, 44300 Nantes, France*

⁸ *INRA, USC 1408 AFMB, F-13288 Marseille, France*

⁹*Department of Biological Sciences, King Abdulaziz University, Jeddah, Saudi Arabia*

¹⁰*Department of Microbiology and Immunology, University of Michigan Medical School, Ann Arbor, MI, USA*

¶These authors contributed equally.*To whom correspondence should be addressed:
D. Wade Abbott (wade.abbott@agr.gc.ca); Harry J. Gilbert (harry.gilbert@ncl.ac.uk),

39 The major nutrients available to human colonic *Bacteroides* species are
40 glycans exemplified by pectins, a network of covalently linked plant cell wall
41 polysaccharides containing galacturonic acid (GalA). Metabolism of complex
42 carbohydrates by the *Bacteroides* genus is orchestrated by polysaccharide
43 utilisation loci or PULs. In *Bacteroides thetaiotaomicron*, a human colonic
44 bacterium, the PULs activated by the different pectin domains have been
45 identified, however, the mechanism by which these loci contribute to the
46 degradation of these GalA-containing polysaccharides is poorly understood.
47 Here we show that each PUL orchestrates the metabolism of specific pectin
48 molecules, recruiting enzymes from two previously unknown glycoside
49 hydrolase (GH) families. The apparatus that depolymerizes the backbone of
50 rhamnogalacturonan-I (RGI) is particularly complex. This system contains
51 several GHs that trim the remnants of other pectin domains attached to RGI,
52 while nine enzymes contribute to the degradation of the backbone comprising
53 a rhamnose-GalA repeating unit. The catalytic properties of the pectin
54 degrading enzymes are optimized to protect the glycan cues that activate the
55 specific PULs ensuring a continuous supply of inducing molecules throughout
56 growth. The contribution of *Bacteroides* spp. to the metabolism of the pectic
57 network is illustrated by cross-feeding between organisms.

58
59 The human gut microbiota (HGM) impacts on host physiology and health^{1,2}.
60 Understanding the mechanisms of nutrient acquisition by the HGM, exemplified by
61 glycan metabolism³⁻⁵, underpins the development of probiotic and prebiotic
62 strategies that maximize human health. While glycan acquisition by human colonic
63 *Bacteroides* species is well established⁶⁻⁹, it should be emphasised that Firmicutes
64 are more abundant in the HGM of Western populations, however, the mechanism by
65 which they metabolise complex carbohydrates is less well understood³. Indeed, it is
66 likely that Firmicutes make a substantial contribution to the degradation of dietary
67 and host glycans in the HGM. The glycan degrading systems of *Bacteroidetes* are
68 encoded by polysaccharide utilization loci (PULs) that are activated by the target
69 carbohydrate³. These systems comprise surface glycan binding proteins (SGBPs),
70 outer membrane oligosaccharide transporters; SusC and SusD homologues (SusC_H
71 and SusD_H, respectively), and surface and periplasmic carbohydrate active enzymes
72 (CAZymes) that are grouped into sequence based families in the CAZy database¹⁰.
73 Relevant to this work are glycoside hydrolase (GH) and polysaccharide lyase (PL)
74 families¹¹.

75
76 Pectins are D-galacturonic acid (D-GalA) rich plant cell wall polysaccharides that are
77 abundant in fruits and vegetables. The two major pectins (see¹² for review) are
78 homogalacturonan (HG) and rhamnogalacturonan-I (RGI) (**Fig. 1a**). HG comprises

79 α -1,4-linked D-GalA and the backbone of RGI is a repeating unit of the disaccharide
80 α -1,2-L-rhamnose (Rha)- α -1,4-D-GalA. Depending on the plant species, the RGI
81 backbone is decorated with galactans (β -1,4-D-galactose (D-Gal) units) and/or
82 arabinans (α -1,5-linked L-arabinofuranose (L-Araf) units with additional L-Araf side-
83 chains)¹³. The backbones of HG and RGI are covalently linked¹⁴. Although individual
84 microbial pectin degrading enzymes have been described¹⁵, the mechanism by
85 which these biocatalysts participate in the concerted degradation of intact pectin
86 remains opaque. *Bacteroides thetaiotaomicron*, a member of the HGM, utilizes all
87 known pectins structures and discreet PULs activated by these glycans have been
88 identified¹⁶. Here we have characterized the function of PULs associated with pectin
89 metabolism, and explored how they contribute to interactions within the HGM
90 foodweb. The data show how these loci coordinate the complex degradative
91 interactions between the backbone and oligosaccharide decorations of these acidic
92 polysaccharides.

93

94 **Results**

95 **The PULs that orchestrate pectin degradation.** Transcriptomic data¹⁶ revealed the
96 PULs upregulated in response to arabinan (*bt0348-bt0369*, Ara-PUL), galactan
97 (*bt4667-bt4673*, Gal-PUL), RGI backbone (*bt4145-bt4183*, RGI-PUL) and HG
98 (*bt4108-bt4124*, HG-PUL) (**Fig. 1b**). To determine the mechanisms by which these
99 loci mediate pectin degradation, the biochemical functions of recombinant proteins
100 encoded by the PULs were determined (**Supplementary Tables 1-5**).

101

102 **Cell surface degradation, substrate binding and import.** Initial degradation of the
103 pectins by *B. thetaiotaomicron* is mediated by endo-acting CAZymes on the surface
104 of the bacterium (**Fig. 2c** and **Supplementary Fig. 1**). These enzymes are essential
105 for pectin utilization as they generate glycans with an appropriate degree of
106 polymerization (DP) for transport into the periplasm¹⁷. Consistent with this premise,
107 deletion of the genes encoding the single outer membrane endo-acting enzymes
108 encoded by RGI-PUL (BT4170) and Gal-PUL (BT4668), **Supplementary Fig. 2** and
109 **Fig. 2c**, prevented growth on the respective pectin (**Fig. 2a**). The surface location of
110 these enzymes was consistent with whole cell assays of *B. thetaiotaomicron* under
111 aerobic conditions (**Fig. 2b**), which report only the activity of surface proteins. To

112 explore the function of the rhamnogalacturonan lyase BT4170, a key component of
113 the RGI degrading apparatus, the crystal structure of the enzyme was determined in
114 complex with ligands. The data (**Supplementary Fig. 3**) showed that the catalytic
115 apparatus of BT4170 and a HG lyase (Pel9A, 1RU4) both located in family PL9,
116 comprising a Brønsted base (Lys285 in BT4170) and a calcium, was conserved.
117 Specificity determinants were identified in subsites distal to the active site, explaining
118 why Pel9A and BT4170 target distinct substrates (see **Supplementary Discussion**
119 and **Supplementary Fig. 3**).

120

121 Ara-PUL and HG-PUL each encode two surface enzymes. The enzymes derived
122 from Ara-PUL, BT0360 and BT0367, are α 1,5-arabinanases that display endo- and
123 endo-processive activity, respectively (**Supplementary Fig. 4** and **Supplementary**
124 **Discussion**). Only $\Delta bt0367$ led to the loss of the arabinan utilization phenotype (**Fig.**
125 **2a**). Gene deletion studies showed that of the two surface PLs (BT4116 and
126 BT4119, **Supplementary Fig. 4** and **Supplementary Table 2**) encoded by HG-PUL,
127 only BT4116 was essential for growth on HG (**Fig. 2a**). The functional significance of
128 BT0360 and BT4119 are unclear, but may reflect the targeting of substrates not
129 evaluated here.

130

131 Gene deletion studies explored the functional significance of the SusC_H/SusD_H pairs
132 encoded by each pectin PUL (**Supplementary Fig. 5**). In HG-PUL, which contains
133 two SusC_H/SusD_H pairs, only the $\Delta bt4114$ mutant displayed no growth on HG,
134 indicating that BT4114 plays a key role in the import of this pectic glycan. Similarly,
135 the Ara-PUL encodes two pairs of SusC_H/SusD_H transporters (BT0361/BT0362 and
136 BT0363/BT0364)¹⁶. Deletion of *bt0364*, but not *bt0362*, prevented growth on
137 arabinan. This indicates that only the BT0363/BT0364 complex is capable of
138 transporting arabinooligosaccharide products. The rationale for the presence of two
139 SusC_H/SusD_H pairs in the HG-PUL and Ara-PUL remains unknown, but likely
140 increases access to additional pectins.

141

142 SGBPs contribute to glycan degradation by bringing substrates into proximity of
143 membrane bound enzymes⁷. Here a single SGBP encoded by each PUL was
144 identified and shown to be specific for the target polysaccharide (**Supplementary**

145 **Table 5**). Only SusD_{Hs} encoded by Gal-PUL and HG-PUL displayed affinity for their
146 cognate glycans (**Supplementary Table 5**). The lack of glycan recognition by
147 SusD_{Hs} associated with the arabinan and RGI degrading systems suggests that the
148 corresponding SusC_H partner is required for ligand recognition. Recent structural
149 data demonstrate that the tight association of SusC_H-D_H pairs¹⁸, supporting the
150 concept that initial ligand recognition can require participation of both protein
151 partners.

152

153 **Periplasmic degradation of pectins.** The oligosaccharides imported into the
154 periplasm were degraded by GHs and PLs. The oligosaccharides generated from
155 galactan and arabinan were depolymerized exclusively by exo-GHs, with HG and the
156 RGI backbone by endo-PLs and exo-GHs (**Supplementary Fig. 2 and 6**).

157

158 With respect to galactan degradation only a single GH2 β 1,4-galactosidase (BT4667)
159 depolymerized galactooligosaccharides generated by the surface endo-galactanase
160 (**Supplementary Fig. 6 and Supplementary Table 3**). Surprisingly the *Δbt4667*
161 mutant displayed no growth defect on galactan (**Supplementary Fig. 5**). This may
162 reflect an element of redundancy within the large number of predicted *B.*
163 *thetaiotaomicron* β -galactosidases¹⁹.

164

165 Periplasmic degradation of arabinan-derived oligosaccharides was mediated by
166 three exo- α -L-arabinofuranosidases (**Supplementary Fig. 6**). BT0369 removed α -
167 1,2-L-arabinofuranose side chains²⁰. Here we demonstrate the GH51 enzymes
168 BT0348 and BT0368 target arabinan side chains, likely α -1,3-arabinofuranosyl
169 linkages, and the backbone α -1,5-arabinofuranosyl linkages, respectively
170 (**Supplementary Table 4 and Supplementary Fig. 6**). BT0349 released β -L-
171 arabinose from an arabinan derived oligosaccharide (**Supplementary Fig. 7 and**
172 **Supplementary Table 7**). The enzyme reveals a previously unknown GH family now
173 designated GH146 (**Supplementary Fig. 8 and Supplementary Discussion**).

174

175 RGI released from the pectin network contains remnants of arabinan, galactan and
176 HG. Prior to RGI backbone depolymerisation these accessory structures must be
177 removed, explaining why RGI-PUL is so complex. To characterise these accessory

178 enzymes we used RGI from potato galactan (RGI-P), which contains many of these
179 remnants. Galactan substitutions were cleaved from the RGI-P backbone by the
180 synergistic action of three exo- β -1,4-galactosidases, BT4151, BT4156 and BT4160
181 (**Supplementary Table 1**). BT4160 targeted galactooligosaccharides, while the
182 other two enzymes released galactose only from RGI-P. The lack of functional
183 arabinofuranosidase genes in RGI-PUL likely reflects the role of single β 1,4-D-Gal
184 units in linking arabinan chains to the RGI backbone¹³. Enzyme cocktail data indicate
185 that BT4151 and BT4156 play a pivotal role in exposing the backbone of RGI to
186 enzymatic attack (**Supplementary Fig. 9**). RGI-PUL also encodes the esterase
187 BT4158 (**Supplementary Table 1**), which releases acetyl groups from D-GalA in the
188 RGI backbone, was also shown to be important for the depolymerisation of the
189 glycan (**Supplementary Fig. 9**). A GH28 α -D-galacturonidase (BT4155), which
190 targets HG (**Supplementary Table 1**), removed D-GalA from RGI-P but not from the
191 glycan in Arabidopsis mucilage (RGI-AM), which contains no HG decorations. The
192 crystal structure of BT4155 (**Supplementary Fig. 10**) revealed the expected β -helix
193 for a GH28 enzyme²¹. In the center of the helix is a pocket that houses three
194 carboxylate residues that comprise the predicted catalytic apparatus based on
195 conservation with other GH28 enzymes²² and mutagenesis data (**Supplementary**
196 **Table 6**). The pocket extends into a channel-like structure that likely accommodates
197 the conformation adopted by HG but not the RGI backbone.

198

199 In addition to enzymes classically associated with pectin degradation, RGI-PUL
200 encodes BT4157, which is located in the apparent “non-pectinase family” GH27. The
201 enzyme (**Supplementary Table 1**) was shown to be a α -galactosidase, which likely
202 targets single α -galactose units that decorate the RGI backbone from Okra plants²³.
203 Another example of enzyme diversity is the β -D-glucuronidase activity displayed by
204 BT4181 against sugar beet arabinan in which the RGI backbone is known to contain
205 GlcA²⁴ (**Supplementary Fig. 6**). It is evident, therefore, that the pectin degrading
206 systems are able to accommodate diversity in the fine-chemistry of RGI structures
207 from a variety of plants.

208

209 In contrast to exo-cleavage of arabinan and galactan, the backbone of RGI and HG
210 were initially cleaved by endo-PLs and the products depolymerized by exo-GHs (**Fig.**

211 **1** and **Supplementary Fig. 2** and **6**). The different degradative strategy likely reflects
212 the high DP of the imported RGI- and HG-derived oligosaccharides compared to the
213 neutral glycans. Thus, the initial concentration of available substrate for exo-GHs is
214 low, but is increased by the endo-PLs. RGI-PUL encodes three periplasmic PLs,
215 respectively. Of particular note is BT4175, which was shown to accommodate
216 glycans appended to backbone rhamnose units (**Supplementary Fig. 2**), ensuring
217 that cleavage of the (Rha-GalA)_n polymer occurred in concert with, and not
218 subsequent to, side-chain removal.

219

220 The β -elimination of the RGI and HG backbone by the PLs generated Δ 4,5-GalA.
221 The unsaturated residues were removed from RGI oligosaccharides with a DP of 2
222 or ≥ 4 by BT4176 or BT4174, respectively (**Supplementary Table 1**); and HG
223 oligosaccharides by BT4108 (**Supplementary Table 2**), which expands the activity
224 for the GH105 family. BT4108 products were then depolymerized to GalA by the
225 exo- α -galacturonidase BT4123 (**Supplementary Table 2** and **Supplementary Fig.**
226 **6**). The RGI-AM oligosaccharides were degraded through the successive action of a
227 RGI-specific GH106 α -L-rhamnosidase (BT4145) and one of three GH28
228 rhamnogalacturonidases (BT4146, BT4153 and BT4149) that target [D-GalAp- α -1,2-
229 L-Rhap]_n with a DP of 2, ≥ 2 or ≥ 4 , respectively (**Supplementary Table 1**). BT4145
230 cleaved rhamnosidic linkages through an inverting mechanism (**Supplementary Fig.**
231 **11**). The biological rationale for galacturonidases that target substrates with different
232 DPs is unclear. Surprisingly deletion of BT4145 only extended lag phase
233 (**Supplementary Fig. 5**), likely reflecting the slow but complete degradation of RGI-
234 AM by the PLs and Δ 4,5-unsaturated- α -rhamnogalacturonidases.

235

236 **The ligands that activate the pectin degradative system.** Previously
237 arabinooligosaccharides with DP ≥ 6 were shown to activate Ara-PUL¹⁶. Here we
238 determined ligands that bound and activated the hybrid two component system
239 (HTCS) of the pectin PULs. The data (**Supplementary Table 5** and **Supplementary**
240 **Fig. 12**) demonstrate that the HTCS of Ara-PUL bound linear but not decorated
241 arabinan, and the sensor of the Gal-PUL HTCS (BT4673) recognised small
242 galactooligosaccharides. Only the oligosaccharide Δ 4,5GalA- α -1,2-Rha- α -1,4-GalA-
243 α -1,2-Rha, a major limit product of the rhamnogalacturonan lyases, bound the HTCS

244 (BT4178) that regulates RGI-PUL. Saturated RGI oligosaccharides failed to bind the
245 sensor, indicating that unsaturation of the non-reducing terminal sugar is a
246 recognition determinant. The HTCS that unregulates HG-PUL recognised only
247 saturated HG-derived oligosaccharides. The mRNA levels of the *susC_H* genes of the
248 pectin PULs showed that activation of RGI-PUL resulted in a small up-regulation of
249 HG-PUL and RGII-PUL1 (**Supplementary Fig. 13**). This may reflect the need to
250 extract RGI from pectins networks through cleavage of adjacent HG segments, as a
251 prelude to its degradation.

252

253 Exo-acting enzymes that target the remnants of RGI side chains and α -1,3-L-Araf
254 units that decorate arabinan were substantially less active than GHs that
255 depolymerised the backbone of the respective glycans (**Supplementary Tables 1**
256 **and 4**). Additionally, BT4108, which removed 4,5 Δ GalA from HG-oligosaccharides
257 generating the HTCS activating ligand was slow compared to the other enzymes that
258 act on these pectins (**Supplementary Tables 1 and 2**). The biological rationale for
259 this difference in catalytic competence, may reflect the need to protect the inducing
260 ligand (**Fig. 3**), as proposed for the chondroitin sulfate utilization system²⁵. Slow
261 release of the side chain stubs or unsaturated uronic acids will block the rapid
262 degradation of the backbone ensuring that there is continuous production of the
263 activating molecules throughout growth on the respective glycan.

264

265 **Pectin utilization within the HGM *Bacteroidetes* and the extent of cross-** 266 **feeding.**

267 To explore pectin utilization by HGM *Bacteroidetes* growth of the different species on
268 these GalA-rich polysaccharides was determined. The data showed that only *B.*
269 *ovatus*, *B. thetaiotaomicron* and *B. fingoldii* utilised all the pectins, although the
270 majority of other organisms could grow on at least some of these glycans
271 (**Supplementary Fig. 14** and **Supplementary Table 8**). Around 70% of the
272 organisms grew on HG and galactan, while only four *Bacteroides* strains utilise the
273 RGI backbone (RGI-AM). However, 56% and 100% of the strains unable to utilise
274 RGI-AM and potato galactan, respectively, grew on the respective oligosaccharides,
275 demonstrating that these organisms utilise pectin degradation products. A key
276 question is the source of oligosaccharides available to these organisms. Evidence of

277 cross-feeding was provided by mutants of *B. thetaiotaomicron* engineered to utilize
278 only pectic oligosaccharides [lacking the surface endo-galactanase ($\Delta bt4668$) or RGI
279 lyase ($\Delta bt4170$)], which grew on the cognate polysaccharide when co-cultured with
280 wild type *B. thetaiotaomicron* (**Fig. 4a**). These data show that wild type *B.*
281 *thetaitotaomicron* released polysaccharide breakdown products (PBP; **Fig. 2f**) into
282 culture media, which were available to other organisms. This is consistent with *B.*
283 *uniformis* (grows on galactooligosaccharides but not galactan in mono-culture)
284 utilisation of the polysaccharide when co-cultured with wild type *B. thetaiotaomicron*
285 (**Fig. 4b**). This pectin cross-feeding between *B. thetaiotaomicron* and other
286 *Bacteroides* species, however, is variable. Although *B. massiliensis* utilize HG or RGI
287 oligosaccharides, the bacterium failed to grow on the cognate polysaccharides when
288 co-cultured with *B. thetaiotaomicron* (**Fig. 4b**). This likely reflects the large PBPs
289 generated by *B. thetaiotaomicron* from these pectins, while *B. massiliensis* appears
290 to import only RGI and HG oligosaccharides with a low DP. The lack of cross-feeding
291 of some pectin-derived PBPs is evident in arabinan utilization. *B. ovatus* and
292 engineered *B. thetaiotaomicron* ($\Delta bt0360/\Delta bt0367$, lacking the two surface endo-
293 arabinanases) both grew on arabinooligosaccharides but not arabinan. The two
294 organisms, however, failed to utilise arabinan when co-cultured with wild type *B.*
295 *thetaitotaomicron* (**Fig. 4b**). Although *B. thetaiotaomicron* released
296 arabinooligosaccharides (**Fig. 2f**), the high DP of these molecules (reflects slow
297 activity of the surface endo-arabinanases²⁰) may have prevented transport into the
298 periplasm of these organisms.

299

300 **Genetic basis of pectin utilization among the *Bacteroides*.** Loci corresponding to
301 *B. thetaiotaomicron* Gal-PUL in other *Bacteroides* species (**Supplementary Fig. 15**)
302 contained an additional ORF, which, in the *B. ovatus* Gal-PUL, encodes a β -
303 galactosidase (BACOVA_05493) with a retaining mechanism (**Supplementary Fig.**
304 **16**) that belongs to a previously unknown CAZy family (assigned GH147). The
305 enzyme was particularly active against galactohexaose and galactan
306 (**Supplementary Fig. 6** and **Supplementary Table 3**). The importance of this
307 enzyme is illustrated by the severe growth defect displayed by $\Delta bacova_05493$ on
308 galactan (**Fig. 2**). Whole cell assays with galactan revealed the accumulation of
309 galactose and not galactooligosaccharides, as occurs in *B. thetaiotaomicron*,

310 suggesting that BACOVA_05493 is located on the bacterial surface. This was
311 confirmed by whole cell assays of *Δbacova_05493*, which revealed no products were
312 generated from galactan. This not only demonstrates that BACOVA_05493 is a
313 surface enzyme but shows that the endo-galactanase, BACOVA_05488, consistent
314 with its very low activity (**Supplementary Fig. 2**), did not contribute to galactan
315 degradation.

316

317 We examined whether the *B. thetaiotaomicron* pectin PULs provide a genetic model
318 for *Bacteroides* utilisation of these glycans. A 16S-based phylogenetic tree of the
319 *Bacteroides* species was constructed and the organisms labelled for PUL
320 conservation and growth on the respective oligo- and polysaccharides
321 (**Supplementary Fig. 14**). There is $\geq 80\%$ agreement between the presence of a
322 PUL and growth of the bacterium on the corresponding poly- or oligosaccharide.
323 Growth, however, was apparent in some organisms without an equivalent PUL,
324 showing that bacteria can deploy alternative pathways to utilise a particular glycan.
325 There were also examples of the presence of the cognate PUL without growth of the
326 corresponding pectin. PUL conservation was also not always congruent with the
327 16S phylogeny (**Supplementary Fig. 14** and **Supplementary Fig. 15**). Thus, *B.*
328 *ovatus*, *B. xylanisolvens* and *B. caccae* form a monophyletic group yet only *B.*
329 *xylanisolvens* has a galactan PUL, while only *B. caccae* has lost the RGI PUL
330 (**Supplementary Fig. 14**). The arabinan PUL of *B. ovatus* is fragmented and that of
331 *B. caccae* absent (**Supplementary Fig. 15a**). *B. egghertii*, *B. stercoris* and *B. clarus*,
332 also form a monophyletic group, but only *B. stercoris* has conserved the galactan
333 PUL, while *B. eggerthii* has an arabinan PUL but has lost its RGI PUL
334 (**Supplementary Fig. 15d**). A final example involves *B. thetaiotaomicron* and *B.*
335 *xylanisolvens*, which are closely related species, yet have different arabinan PULs.
336 The arabinan PUL of *B. thetaiotaomicron* is identical to *B.*
337 *cellulosilyticus/oleiciplenus/intestinalis*, while the arabinan PUL of *B. xylanisolvens* is
338 similar to *B. egghertii*. Our observations suggest that in the course of evolution
339 *Bacteroides* rapidly gain and lose PULs that target different pectin structures.

340

341 **Discussion**

342 Combining biochemical properties and cellular location of the enzymes that target
343 pectins, with growth profiles of mutants containing gene deletions in the appropriate
344 PULs, enabled models for the metabolism of each pectic substructure, showing how
345 the individual pathways are coordinated by *B. thetaiotaomicron* (**Fig 5**). The data
346 revealed that 30 GHs and PLs are required to degrade the major pectin domains.
347 Given that large numbers of enzymes are also required to degrade starch and the
348 hemicelluloses, it is evident that plant glycan metabolism explains the extremely
349 large repertoire of CAZyme gene clusters in colonic *Bacteroides* species.

350

351 In contrast to several *Bacteroides* glycan degrading systems where the surface GHs
352 act slowly and target infrequent linkages^{7,26,27}, the equivalent enzymes of *B.*
353 *thetaitotaomicron* that cleave galactan and the backbone of HG and RGI rapidly
354 degrade their target polysaccharide. This likely reflects substrate accessibility to
355 enzyme attack, and thus organisms with efficient surface enzymes that target
356 accessible carbohydrates would be more competitive than bacteria in which the
357 corresponding GHs or PLs were inefficient. This model (**Fig. 5**), however, does not
358 apply to arabinan degradation where low activity of the surface enzymes was
359 evident. This observation underpins the distinct mechanisms, distributive or selfish,
360 by which glycans are metabolized by *Bacteroides* spp.

361

362 The RGI-PUL, in addition to orchestrating RGI backbone depolymerisation, removes
363 remnants of linked polysaccharides and single sugar sidechains (**Fig. 5**). In contrast,
364 PULs that mediate degradation of other branched glycans^{7,8,26,27} depolymerize both
365 the respective side chains and backbone structures. We propose that *B.*
366 *thetaitotaomicron* does not necessarily target intact pectin structures but are able to
367 utilise pectin domains generated by other organisms in the HGM. The RGI backbone
368 exposed through symbiotic relationships with other intestinal microorganisms, or
369 upstream processing by other PULs of *B. thetaiotaomicron*, is likely to contain
370 additional pectin remnants explaining the complexity of enzymes encoded by the
371 RGI-PUL.

372

373

374 The cross-feeding experiments demonstrate that galactooligosaccharides released
375 by *B. thetaiotaomicron* are used by other organisms. The utilization of other pectin-

376 derived PBPs, however, is more restricted. These data illustrate how glycans are
377 made available to the general community by primary degraders. Such cross-feeding
378 has been observed between strains of *Bacteroides* cultured on fructans and soluble
379 starch²⁸, with the recipient organism providing a benefit to the glycan degrading
380 bacterium²⁹. Possible non-*Bacteroides* beneficiaries of pectin-derived cross-feeding
381 within the HGM are *Bifidobacterium* species, which generally utilize PBPs rather than
382 the polysaccharide²⁷. Contrasting oligosaccharide utilisation profiles observed
383 among *Bacteroides spp.* may allow for co-existence of species within the same niche
384 targeting different components of the same glycans without competition.

385

386 The critical role played by a surface exo- β -galactosidase in galactan metabolism in
387 some *Bacteroides* species is intriguing. This contrasts with all other *Bacteroides*
388 glycan degrading systems described to date, which deploy endo-acting
389 CAZymes^{2,7,8,27,30}. These organisms may target galactooligosaccharides, albeit with
390 a high DP, released by other organisms within the HGM, obviating that need for
391 endo-cleavage. This indicates that different *Bacteroides* target galactans in distinct
392 nutritional niches within the gut. The data also illustrate the risk associated with
393 generating models for glycan degradation based solely on prediction of enzyme
394 function through CAZy family assignment. To fully understand glycan metabolism a
395 molecular genetics approach informed by biochemical and transcriptional data in
396 harness with bioinformatics predictions is required.

397

398 This report provides a model for how the pectic network is metabolized by a
399 *Bacteroides* species in the HGM. Surprising variations in selective glycan
400 metabolism and the constitution of individual pathways were apparent. This contrasts
401 with the extensive conservation of other PULs^{7-9,27}. This suggests that organisms
402 have adopted a variety of strategies to metabolise dietary pectins. A salient feature
403 of pectin utilization is the elaboration of enzymes in the RGI-PUL, reflecting the
404 requirement to remove remnants from other pectic glycans and the extraordinary
405 number of enzymes deployed in depolymerizing the disaccharide backbone.
406 Dissecting the mechanism of pectin degradation contributes to our understanding of
407 the foodweb within the HGM.

408

409 **Methods**

410 **Producing recombinant proteins**

411 DNA fragments encoding predicted CAZymes and binding proteins were amplified
412 without signal sequence by PCR using appropriate primers. The resultant DNA was
413 then cloned into pET21a or pET28a/b linearized using appropriate restriction
414 enzymes. The expressed protein included a His6-tag fusion at the N-terminus.
415 *Escherichia coli* strains BL21(DE3) or TUNER were transformed with the plasmids
416 and grown to mid-exponential phase before induction with 1 mM (BL21(DE3)) or
417 0.2 mM (TUNER) isopropyl β -D-galactopyranoside (IPTG), and the culture was
418 grown for a further 5 h at 37 °C or 16 h at 16 °C, respectively. The recombinant
419 proteins were purified to >90% electrophoretic purity by immobilized metal ion affinity
420 chromatography (IMAC) using Talon, a cobalt-based matrix, with bound proteins
421 eluted with 100 mM imidazole, describe previously ⁹. To generate seleno-methionine
422 (Se-Met) proteins for structure resolution, *E. coli* cells were cultured as described
423 previously ⁹, and the proteins were purified using IMAC as described above. For
424 crystallization, the Se-Met proteins were further purified by size exclusion
425 chromatography. After IMAC, fractions containing the purified proteins were buffer-
426 exchanged, using PD-10 Sephadex G-25M gel-filtration columns (GE Healthcare),
427 into 10 mM Na-HEPES buffer, pH 7.5, containing 150 mM NaCl and were then
428 subjected to gel filtration using a HiLoad 16/60 Superdex 75 column (GE Healthcare)
429 at a flow rate of 1 ml min⁻¹. For crystallization trials, purified proteins were
430 concentrated using an Amicon 10-kDa molecular mass centrifugal concentrator and
431 washed three times with 5 mM DTT (for the Se-Met proteins) or water (for native
432 proteins).

433

434 **Site-directed mutagenesis**

435 Site-directed mutagenesis was carried out employing a PCR-based NZY-
436 Mutagenesis kit (NZYTech Ltd) using the plasmids encoding the appropriate
437 enzymes as the template. The mutated DNA clones were sequenced to ensure that
438 only the appropriate DNA change was introduced after the PCR.

439

440 **Purification of oligosaccharides**

441 Galactooligosaccharides were generated by incubation of 3 g of galactan with 100
442 mM HCl incubated for 3 h at 100 °C and neutralised by NaOH titration. The
443 oligosaccharide mixture was freeze dried and resuspended in water before being
444 applied to a P2-BioGel (BioRad) column with a 0.22 ml/min flow rate. Fractions were
445 evaluated for oligosaccharide content and purity by TLC. Pure fractions of defined
446 oligosaccharides were pooled and concentrated. Oligosaccharide size was
447 confirmed by Mass Spectrometry and HPAEC. Crude oligosaccharide mixtures were
448 generated by partial digestion with appropriate enzymes; BT0360 and BT0367
449 (arabinan), BT4668 (galactan), BT4170 (P-RGI/AM-RGI) and BT4116 (HG).
450 Reactions were boiled and filter sterilised to remove precipitate before being
451 evaluated by TLC.

452

453 **Preparation of RGI-AM**

454 *Arabisopsis thaliana* seeds were resuspended in distilled water (1 g/ml) and
455 incubated at 4 °C for 16 h while stirring. The solution was centrifuged and
456 supernatant filtered through G1 glass filter (15-40 µm pore size). This was then
457 dialysed against 2 x 40 volumes of water before freeze drying. Typical yield was 1 g
458 from 80 g seeds.

459

460 **CAZyme Assays**

461 Spectrophotometric quantitative assays for the □-L-rhamnosidase BT4145, L-
462 arabinofuranosidases (BT0349, BT0348 and BT0368), □-D-galactosidases (BT4667,
463 BT4151, BT4156, BT4160 and BACOVA_05493) and carbohydrate esterase
464 (BT4158) were monitored by the formation of NADH, at $A_{340\text{ nm}}$ using an extinction
465 coefficient of $6,230\text{ M}^{-1}\text{ cm}^{-1}$, with an appropriately linked enzyme assay system.
466 The assays were adapted from purchased Megazyme International assay kits.
467 These kits were as follows: the L-rhamnose assay kit (K-RHAMNOSE); L-
468 arabinose/D-galactose assay kit (K-ARGA); acetic acid detection kit (K-ACET).
469 Activity of pectic lyases (BT4170, BT4175, BT4115, BT4116) were measured at
470 $A_{235\text{ nm}}$. Activity on 4-nitrophenyl-glycosides was monitored at $A_{400\text{ nm}}$. The activity of
471 BT4668 to hydrolyse galactan was determined in 20 mM sodium phosphate buffer,
472 pH 7.5 at 37 °C containing an appropriate concentration of the polysaccharide and
473 1 mg ml^{-1} BSA. Reactions were incubated at 37 °C and at regular time intervals

474 500 μ l aliquots were removed and the amount of reducing sugar was quantified using
475 the dinitrosalicylic acid reagent ³¹ and a standard curve of xylose in the reaction
476 conditions used. Substrate depletion assays were performed as described previously
477 ⁷ to determine BT4668 activity on galactooligosaccharides while production of D-
478 galactose was used to assay BT4160 activity on galactooligosaccharides. The mode
479 of action of enzymes were determined using PAEC or TLC, as appropriate. In brief,
480 aliquots of the enzyme reactions were removed at regular intervals and, after boiling
481 for 10 min to inactivate the enzyme and centrifugation at 13,000g, the amount of
482 substrate remaining or product produced was quantified by HPAEC using standard
483 methodology. The reaction substrates and products were bound to a Dionex
484 CarboPac PA100 (Galactooligosaccharides/Arabinooligosaccharides), PA1
485 (Monosaccharides) or PA20 (Polygalacturonic acid oligosaccharides) column and
486 glycans eluted with an initial isocratic flow of 100 mM NaOH then a 0–200 mM
487 sodium acetate gradient in 100 mM NaOH at a flow rate of 1.0 ml min⁻¹, using pulsed
488 amperometric detection. Linked assays were checked to make sure that the relevant
489 enzyme being analysed was rate limiting by increasing its concentration and
490 ensuring a corresponding increase in rate was observed. A single substrate
491 concentration was used to calculate catalytic efficiency (k_{cat}/K_M), and was checked to
492 be markedly less than K_M by halving and doubling the substrate concentration and
493 observing an appropriate increase or decrease in rate. The equation
494 $V_0 = (k_{cat}/K_M)[S][E]$ was used to calculate k_{cat}/K_M unless substrate depletion was used
495 then the calculation was as follows $\ln(k_{cat}/K_M) = (S_0/S_t)/[E]$, in which $[E]$ and $[S]$ are
496 enzyme and substrate concentration, respectively. All reactions were carried out in
497 20 mM sodium phosphate buffer, pH 7.0, with 150 mM NaCl (defined as standard
498 conditions) and performed in at least technical triplicates.

499

500 **Isothermal Titration Calorimetry**

501 The binding of proteins to their glycan ligands was quantified by isothermal titration
502 calorimetry (ITC), as described previously²⁷. Titrations were carried out in 50 mM Na-
503 HEPES buffer, pH 7.5 at 25 °C. The reaction cell contained protein at 50–100 μ M,
504 while the syringe contained either the oligosaccharide at 1–10 mM or the
505 polysaccharide at 3–10 mg ml⁻¹. Integrated heats were fitted to a single-site model
506 using Microcal Origin v7.0 to derive n , K_a , and ΔH values. ΔG and ΔS were

507 calculated from the equation $-RT\ln K_a = -\Delta G = \Delta H - T\Delta S$ where R is the gas constant
508 and T temperature in Kelvins.

509

510 **Electrospray ionisation mass spectrometry (ESI-MS)**

511 The molecular mass of purified oligosaccharides (in 10 mM ammonium acetate, pH
512 7.0) were analysed via negative ion mode infusion/offline ESI-MS following dilution
513 (typically 1:1 (v/v)) with 5% trimethylamine in acetonitrile.

514

515 Electrospray data was acquired using an LTQ-FT mass spectrometer (Thermo) with
516 a FT-MS resolution setting of 100,000 at $m/z = 400$ and an injection target value of
517 1,000,000. Infusion spray analyses were performed on 5–10 μl of samples using
518 medium 'nanoES' spray capillaries (Thermo) for offline nanospray mass
519 spectrometry in negative ion mode at 1 kV.

520

521 **$^1\text{H-NMR}$ determination of catalytic mechanism**

522 Enzymes BT4145 and BACOVA_05493 were freeze dried in 20 mM Tris-HCl, 500
523 mM NaCl, pH 7.5 as were substrates $\alpha\text{-L-Rha-}\alpha\text{1,4-D-GalA}$ and $(\beta\text{1,4-Galp-})_3$,
524 respectively and resuspended in deuterium oxide. Prior to addition of enzyme an
525 initial $^1\text{H-NMR}$ spectra was obtained. Enzyme was added and spectra recorded at
526 appropriate time intervals. The ratio of $\alpha\text{-}$ and $\beta\text{-}$ monosaccharide products was
527 determined to deduce catalytic mechanism.

528

529 **2D NMR of arabinotetraose before and after treatment with BT0349**

530 NMR spectra were recorded at 298 K in D_2O with a Bruker AVANCE III spectrometer
531 operating at 600 MHz equipped with a TCI CryoProbe. Two-dimensional $^1\text{H-}^1\text{H}$
532 TOCSY, ROESY, DQFCOSY, ^{13}C HSQC and HSQC-TOCSY experiments were
533 performed, using established methods³²; the mixing times were 70 ms and 200 ms
534 for the TOCSY and ROESY experiments, respectively. Chemical shifts were
535 measured relative to internal acetone ($\delta_{\text{H}} = 2.225$, $\delta_{\text{C}} = 31.07$ ppm). Data were
536 processed using the Azara suite of programs (v. 2.8, copyright 1993-2017, Wayne
537 Boucher and Department of Biochemistry, University of Cambridge, unpublished)
538 and chemical-shift assignment was performed using Analysis v2.4³³.

539

540 **Growth of Bacteroides and generation of mutants**

541 *Bacteroides* mutants were generated by deletion or replacement of the target gene
542 with an inactive version by counter selectable allelic exchange using the pExchange-
543 tdk plasmid. The full method is described in³⁴. Mutants generated in this study are
544 distinguished by the locus tag of the gene deleted/inactivated ($\Delta btxxx$ or
545 $\Delta BACOVAxxxxx$).

546

547 *Bacteroides spp.* were routinely cultured under anaerobic conditions at 37 °C using
548 an anaerobic cabinet (Whitley A35 Workstation; Don Whitley) in culture volumes of
549 0.2, 2 or 5 ml) of TYG (tryptone-yeast extract-glucose medium) or minimal medium
550 (MM) containing 0.5-1% of an appropriate carbon source and 1.2 mg ml⁻¹ porcine
551 haematin (Sigma-Aldrich) as previously described⁸. The growth of the cultures were
552 routinely monitored at OD_{600 nm} using a Biochrom WPA cell density meter for the 5 ml
553 cultures or a Gen5 v2.0 Microplate Reader (Biotek) for the 0.2 and 2 ml cultures.

554

555 **Protein cellular localisation**

556 Cellular localization of proteins was carried out as described previously⁷. In brief, *B.*
557 *thetaiotaomicron* cultures were grown overnight (OD_{600 nm} value of 2.0) in 5 ml MM
558 containing 0.5 % potato rhamnogalacturonan I (P-RGI) or homogalacturonan. The
559 next day, cells were collected by centrifugation at 5,000g for 10 min and
560 resuspended in 2 ml PBS. Proteinase K (0.5 mg ml⁻¹ final concentration) was added
561 to 1 ml of the suspension and the other half left untreated (control). Both samples
562 were incubated at 37 °C overnight followed by centrifugation (5,000g for 10 min) to
563 collect cells. To eliminate residual proteinase K activity, cell pellets were
564 resuspended in 1 ml of 1.5 M trichloroacetic acid and incubated on ice for 30 min.
565 Precipitated mixtures were then centrifuged (5,000g, 10 min) and washed twice in
566 1 ml ice-cold acetone (99.8%). The resulting pellets were allowed to dry in a 40 °C
567 heat block for 5 min and dissolved in 250 µl Laemmli buffer. Samples were heated for
568 5 min at 98 °C and mixed by pipetting several times before resolving by SDS-PAGE
569 using 12% gels. Electrophoresed proteins were transferred to nitrocellulose
570 membranes by Western blotting followed by immunochemical detection using
571 primary rabbit polyclonal antibodies (Eurogentec) generated against various proteins
572 and secondary goat anti-rabbit antibodies (Santa Cruz Biotechnology). For BT4119
573 the anti-sera failed to produce the desired reactivity. Thus, a C-terminal Flag peptide

574 (DYKDDDDK) was incorporated at the C-terminals of the native proteins expressed
575 by *B. thetaiotaomicron* through counter-selectable allelic exchange³⁴. This allowed
576 for their detection using rabbit anti-Flag antibodies (Sigma) as primary antibodies. In
577 the case of BT4668, BT0360 and BT0367 mutations (that lead to the inactivation of
578 the encoded enzymes) were made in each gene within the *B. thetaiotaomicron*
579 genome to generate the mutants $\Delta bt4668$, $\Delta bt0360$, $\Delta bt0367$ and $\Delta bt0360/\Delta bt0367$.
580 Cells were grown in MM containing 0.5% arabino- or galacto-oligosaccharides to
581 activate the target PULs. The cells were harvested from mid-log phase 5 ml cultures
582 and concentrated in 0.5 ml PBS. The resuspended cells were incubated with the
583 target glycans in an aerobic environment, conditions in which only the activity of only
584 the surface enzymes can be monitored. The appropriate time intervals samples were
585 taken, subjected to HPAEC analysis. The data were compared to that of wild type *B.*
586 *thetaiotaomicron* to explore whether the loss in enzyme activity occurred at the
587 bacterial surface.

588

589 **Cross-feeding and competition assays**

590 Prior to co-culture each *Bacteroides spp.* was grown in TYG and washed in PBS
591 before being used to inoculate MM containing 0.5% glycan. Samples of 0.5 ml were
592 taken at regular intervals during growth, which were serially diluted and plated onto
593 Brain-Heart Infusion (BHI, Sigma-Aldrich) with agar and porcine hematin for
594 determination of total CFU/ml of the culture. Genomic DNA was purified from the
595 remainder of the sample (Bacterial genomic DNA purification kit, Sigma-Aldrich).
596 Quantitate PCR was used to determine the ratio of different *Bacteroides spp.* or
597 mutants in the sample using primers specific for unique regions in each *Bacteroides*
598 *sp.* genome or tag introduced into one of two *att* sites. The Ratio of each
599 species/mutant was used to calculate the CFU/ml of each organisms in the culture.

600

601 **Quantitative RT-PCR (RT-qPCR)**

602 Comparison of the levels of transcription of *susC* homologues (*susC_H*) from each of
603 the pectin PULs was performed by RT-qPCR. Previous studies have shown *susC_H*
604 genes are a good proxy for expression of their cognate PUL³⁵. *B. ovatus* was
605 cultured in 5 ml of MM containing 0.5% (w/v) carbon source, as described above.
606 Triplicate bacterial cultures were harvested at mid-log phase (OD₆₀₀ ~0.8) and
607 placed in RNAprotect (Qiagen), then stored at -80 °C overnight, before purification

608 with RNeasy kit (Qiagen). RNA purity was assessed spectrophotometrically, and
609 1 µg of RNA was used immediately for reverse transcription (QuantiTect Reverse
610 Transcription kit, Qiagen). RT-qPCR was performed in a 96-well plate on a
611 LightCycler 480 System (Roche) with FastStart Essential DNA Green Master
612 (Roche) using the standard primer. Reactions were carried out in 10 µl, consisting of
613 5 µl SYBR Green mix, 20 ng of cDNA, and 1 µM (*susC_H* genes) or 0.125 µM (16 S
614 rRNA) primer mix. Reaction conditions were 95 °C 600 s, followed by 45 cycles of
615 95 °C for 10 s, 55 °C for 10 s, 72 °C for 10 s. Cq values were calculated using
616 LightCycler 480 SW 1.5. Data were normalized to 16 S rRNA transcript levels, and
617 change in expression level calculated as fold-change compared with minimal media,
618 glucose cultures.

619

620 **Crystal structure determination**

621 **Crystallisation:** All proteins were concentrated to 10 mg/ml. BT4170 native
622 crystallised in 20 mM sodium/potassium phosphate 20% (w/v) polyethylene glycol
623 (PEG) 3350. BT4170 co-crystallised with 10 mM of oligosaccharide reaction
624 products generated by BT4170 (defined as ligand) in 100 mM succinic acid, sodium
625 phosphate glycine buffer at pH 6.0 and 25 % (w/v) PEG 1500. BT4170 inactive
626 mutant K285A was co-crystalized with 30 mM ligand in 200 mM potassium chloride
627 and 20% PEG 3350. Selenomethionine-containing BT4155 crystalized in 200 mM
628 sodium chloride, 100 mM Bis-Tris buffer pH 5.5 and 25% PEG 3350. BT0349 with
629 500 mM L-arabinose was crystallised in 20 % PEG 3350 and 200 mM ammonium
630 formate. All samples were cryo-protected by supplementing the mother liquor with
631 20% PEG 400.

632

633 **Data collection and processing:** BT0349, BT4170 and BT4170 K285A ligand data
634 were indexed and integrated with the automated pipeline Xia2 (3da protocol)³⁶.
635 BT4170 in complex with ligand and BT4155 were indexed and integrated with XDS³⁷.
636 The data were scaled with either XDS or Aimless³⁸. Space group determination was
637 confirmed with Pointless³⁹. The phase problem for BT0349 and BT4155 was solved
638 by SeMet-SAD using hkl2map⁴⁰ and the shelx pipeline⁴¹. BT4170 native apo data
639 were solved by molecular replacement with the pipeline Balbes⁴² with the PDB
640 model 1RU4 as search model. Initial models of BT0349, BT4155 and BT4170 were
641 improved by successive runs of automated model building program arp_warp⁴³ and

642 buccaneer⁴⁴. BT4170 TRI SCACCHARIDE and BT4170 inactive mutant K285A data
643 were solved using the 4170 native apo model. All models were refined and improved
644 using successive cycle of Refmac⁴⁵ and manual model building with Coot⁴⁶. All
645 models were validated using Coot⁴⁶ and molprobity⁴⁷. Five percent of the
646 observations were randomly selected for the Rfree set. The data processing,
647 refinement statistics and protein database (PDB) codes are reported in
648 **Supplementary Table 9**

649

650 **Comparative genomics analysis**

651 PULs similar to the RGI, galactan, arabinan and homogalacturonan PULs were
652 searched in HGM Bacteroidetes genomes. The identification of similar PULs was
653 based on PUL alignments. Gene composition and order of Bacteroidetes PULs were
654 computed using the PUL predictor described in PULDB⁴⁸. Then, in a manner similar
655 to amino acid sequence alignments, the predicted PULs were aligned to the
656 appropriate pectin PULs according to their modularity as proposed in the
657 RADS/RAMPAGE method⁴⁹. Modules taken into account include CAZy families,
658 sensor-regulators and *suscd*-like genes. Finally, PUL boundaries and limit cases
659 were refined by BLASTP-based analysis. The previously unknown glycoside
660 hydrolase families discovered in this study are listed in the main text.

661

662 **Data availability.** The data that support the findings of this study are available from
663 the corresponding author upon request. The authors declare that the data supporting the
664 findings of this study are available within the paper and the Supplementary Information.
665 Complete western blot images are provided in **Supplementary Fig. 1**. The crystal
666 structure datasets generated (coordinate files and structure factors) have been deposited in
667 the Protein Data Bank (PDB) and are listed in **Supplementary Table 9** together with the
668 PDB accession codes.

669

670 **REFERENCES**

671

- 672 1 Gilbert, J. A. *et al.* Microbiome-wide association studies link dynamic microbial
673 consortia to disease. *Nature* **535**, 94-103, (2016).
- 674 2 Sonnenburg, J. L. & Backhed, F. Diet-microbiota interactions as moderators
675 of human metabolism. *Nature* **535**, 56-64, (2016).
- 676 3 Koropatkin, N. M., Cameron, E. A. & Martens, E. C. How glycan metabolism
677 shapes the human gut microbiota. *Nat Rev Microbiol* **10**, 323-335, (2012).
- 678 4 Desai, M. S. *et al.* A Dietary Fiber-Deprived Gut Microbiota Degrades the
679 Colonic Mucus Barrier and Enhances Pathogen Susceptibility. *Cell* **167**, 1339-
680 1353 e1321, (2016).

- 681 5 Wu, M. *et al.* Genetic determinants of in vivo fitness and diet responsiveness
682 in multiple human gut Bacteroides. *Science* **350**, aac5992, (2015).
- 683 6 Cartmell, A. *et al.* How members of the human gut microbiota overcome the
684 sulfation problem posed by glycosaminoglycans. *Proc Natl Acad Sci U S A*
685 **114**, 7037-7042, (2017).
- 686 7 Cuskin, F. *et al.* Human gut Bacteroidetes can utilize yeast mannan through a
687 selfish mechanism. *Nature* **517**, 165-169, (2015).
- 688 8 Larsbrink, J. *et al.* A discrete genetic locus confers xyloglucan metabolism in
689 select human gut Bacteroidetes. *Nature* **506**, 498-502, (2014).
- 690 9 Ndeh, D. *et al.* Complex pectin metabolism by gut bacteria reveals novel
691 catalytic functions *Nature* **544**, 65-70, (2017).
- 692 10 Lombard, V., Golaconda Ramulu, H., Drula, E., Coutinho, P. M. & Henrissat,
693 B. The carbohydrate-active enzymes database (CAZy) in 2013. *Nucleic Acids*
694 *Res* **42**, D490-495, (2014).
- 695 11 Gilbert, H. J. The biochemistry and structural biology of plant cell wall
696 deconstruction. *Plant Physiol* **153**, 444-455, (2010).
- 697 12 Caffall, K. H. & Mohnen, D. The structure, function, and biosynthesis of plant
698 cell wall pectic polysaccharides. *Carbohydr Res* **344**, 1879-1900, (2009).
- 699 13 Lau, J. M., Mcneil, M., Darvill, A. G. & Albersheim, P. Treatment of
700 Rhamnogalacturonan-I with Lithium in Ethylenediamine. *Carbohydr Res* **168**,
701 245-274, (1987).
- 702 14 Coenen, G. J., Bakx, E. J., Verhoef, R. P., Schols, H. A. & Voragen, A. G. J.
703 Identification of the connecting linkage between homo- or xylogalacturonan
704 and rhamnogalacturonan type I. *Carbohydr Polym* **70**, 224-235, (2007).
- 705 15 Bonnin, E., Garnier, C. & Ralet, M. C. Pectin-modifying enzymes and pectin-
706 derived materials: applications and impacts. *Appl Microbiol Biotechnol* **98**,
707 519-532, (2014).
- 708 16 Martens, E. C. *et al.* Recognition and degradation of plant cell wall
709 polysaccharides by two human gut symbionts. *PLoS Biol* **9**, e1001221,
710 (2011).
- 711 17 Martens, E. C., Koropatkin, N. M., Smith, T. J. & Gordon, J. I. Complex glycan
712 catabolism by the human gut microbiota: the Bacteroidetes Sus-like paradigm.
713 *J Biol Chem* **284**, 24673-24677, (2009).
- 714 18 Glenwright, A. J. *et al.* Structural basis for nutrient acquisition by dominant
715 members of the human gut microbiota. *Nature* **541**, 407-411, (2017).
- 716 19 Xu, J. *et al.* A genomic view of the human-Bacteroides thetaiotaomicron
717 symbiosis. *Science* **299**, 2074-2076, (2003).
- 718 20 Cartmell, A. *et al.* The structure and function of an arabinan-specific alpha-
719 1,2-arabinofuranosidase identified from screening the activities of bacterial
720 GH43 glycoside hydrolases. *J Biol Chem* **286**, 15483-15495, (2011).
- 721 21 Pickersgill, R., Smith, D., Worboys, K. & Jenkins, J. Crystal structure of
722 polygalacturonase from *Erwinia carotovora* ssp. *carotovora*. *J Biol Chem* **273**,
723 24660-24664, (1998).
- 724 22 van Santen, Y. *et al.* 1.68-angstrom crystal structure of
725 endopolygalacturonase II from *Aspergillus niger* and identification of active
726 site residues by site-directed mutagenesis. *J Biol Chem* **274**, 30474-30480,
727 (1999).
- 728 23 Sengkhamparn, N. *et al.* Okra pectin contains an unusual substitution of its
729 rhamnosyl residues with acetyl and alpha-linked galactosyl groups. *Carbohydr*
730 *Res* **344**, 1842-1851, (2009).

- 731 24 Renard, C. M., Crepeau, M. J. & Thibault, J. F. Glucuronic acid directly linked
732 to galacturonic acid in the rhamnogalacturonan backbone of beet pectins. *Eur*
733 *J Biochem* **266**, 566-574, (1999).
- 734 25 Raghavan, V., Lowe, E. C., Townsend, G. E., 2nd, Bolam, D. N. & Groisman,
735 E. A. Tuning transcription of nutrient utilization genes to catabolic rate
736 promotes growth in a gut bacterium. *Mol Microbiol* **93**, 1010-1025, (2014).
- 737 26 Bagenholm, V. *et al.* Galactomannan catabolism conferred by a
738 polysaccharide utilization locus of *Bacteroides ovatus*: enzyme synergy and
739 crystal structure of a beta-mannanase. *J Biol Chem* **292**, 229-243, (2017).
- 740 27 Rogowski, A. *et al.* Glycan complexity dictates microbial resource allocation in
741 the large intestine. *Nat Commun* **6**, 7481, (2015).
- 742 28 Rakoff-Nahoum, S., Coyne, M. J. & Comstock, L. E. An ecological network of
743 polysaccharide utilization among human intestinal symbionts. *Curr Biol* **24**,
744 40-49, (2014).
- 745 29 Rakoff-Nahoum, S., Foster, K. R. & Comstock, L. E. The evolution of
746 cooperation within the gut microbiota. *Nature* **533**, 255-259, (2016).
- 747 30 Foley, M. H., Cockburn, D. W. & Koropatkin, N. M. The Sus operon: a model
748 system for starch uptake by the human gut Bacteroidetes. *Cell Mol Life Sci*
749 **73**, 2603-2617, (2016).
- 750 31 Miller, G. L. Use of dinitrosalicylic acid reagent for determination of reducing
751 sugar. *Anal. Chem.* **31**, 426-428, (1959).
- 752 32 Cavanagh, J., Fairbrother, W. J., Palmer, A. G. & Skelton, N. J. *Protein NMR*
753 *Spectroscopy: Principles and Practice*. (Academic Press, 1996).
- 754 33 Vranken, W. F. *et al.* The CCPN data model for NMR spectroscopy:
755 development of a software pipeline. *Proteins* **59**, 687-696, (2005).
- 756 34 Koropatkin, N. M., Martens, E. C., Gordon, J. I. & Smith, T. J. Starch
757 catabolism by a prominent human gut symbiont is directed by the recognition
758 of amylose helices. *Structure* **16**, 1105-1115, (2008).
- 759 35 Despres, J. *et al.* Unraveling the pectinolytic function of *Bacteroides*
760 *xylanisolvans* using a RNA-seq approach and mutagenesis. *BMC Genomics*
761 **17**, 147, (2016).
- 762 36 Winter, G. xia2: an expert system for macromolecular crystallography data
763 reduction. *J Appl Crystallogr* **43**, 186-190, (2010).
- 764 37 Kabsch, W. Xds. *Acta Crystallogr D Biol Crystallogr* **66**, 125-132, (2010).
- 765 38 Evans, P. R. & Murshudov, G. N. How good are my data and what is the
766 resolution? *Acta Crystallogr D Biol Crystallogr* **69**, 1204-1214, (2013).
- 767 39 Evans, P. R. An introduction to data reduction: space-group determination,
768 scaling and intensity statistics. *Acta Crystallogr D Biol Crystallogr* **67**, 282-
769 292, (2011).
- 770 40 Pape, T. & Schneider, T. R. HKL2MAP: a graphical user interface for
771 macromolecular phasing with SHELX programs. *J Appl Crystallogr* **37**, 843-
772 844, (2004).
- 773 41 Sheldrick, G. M. Experimental phasing with SHELXC/D/E: combining chain
774 tracing with density modification. *Acta Crystallogr D Biol Crystallogr* **66**, 479-
775 485, (2010).
- 776 42 Long, F., Vagin, A. A., Young, P. & Murshudov, G. N. BALBES: a molecular-
777 replacement pipeline. *Acta Crystallogr D Biol Crystallogr* **64**, 125-132, (2008).
- 778 43 Langer, G., Cohen, S. X., Lamzin, V. S. & Perrakis, A. Automated
779 macromolecular model building for X-ray crystallography using ARP/wARP
780 version 7. *Nat Protoc* **3**, 1171-1179, (2008).

- 781 44 Cowtan, K. Fitting molecular fragments into electron density. *Acta Crystallogr D Biol Crystallogr* **64**, 83-89, (2008).
782
783 45 Vagin, A. A. *et al.* REFMAC5 dictionary: organization of prior chemical
784 knowledge and guidelines for its use. *Acta Crystallogr D Biol Crystallogr* **60**,
785 2184-2195, (2004).
786 46 Emsley, P. & Cowtan, K. Coot: model-building tools for molecular graphics.
787 *Acta Crystallogr D Biol Crystallogr* **60**, 2126-2132, (2004).
788 47 Chen, V. B. *et al.* MolProbity: all-atom structure validation for macromolecular
789 crystallography. *Acta Crystallogr D Biol Crystallogr* **66**, 12-21, (2010).
790 48 Terrapon, N., Lombard, V., Gilbert, H. J. & Henrissat, B. Automatic prediction
791 of polysaccharide utilization loci in Bacteroidetes species. *Bioinformatics* **31**,
792 647-655, (2015).
793 49 Terrapon, N., Weiner, J., Grath, S., Moore, A. D. & Bornberg-Bauer, E. Rapid
794 similarity search of proteins using alignments of domain arrangements.
795 *Bioinformatics* **30**, 274-281, (2014).
796 50 Varki, A. *et al.* Symbol Nomenclature for Graphical Representations of
797 Glycans. *Glycobiology* **25**, 1323-1324, (2015).

798

799 **Correspondence and requests for materials should be addressed to H.J.G.**

800 **Acknowledgements**

801 This work was supported in part by an Advanced Grant from the European Research
802 Council (Grant No. 322820) awarded to H.J.G. and B.H. supporting A.S.L., D.N., A.C. and
803 N.T., a Wellcome Trust Senior Investigator Award to HJG (grant No. WT097907MA) that
804 supported J.B. and E.C.L. a European Union Seventh Framework Initial Training Network
805 Programme entitled the "WallTraC project" (Grant Agreement number 263916) awarded to
806 M-C.R. and H.J.G, which supported X.Z. and J.S. The Biotechnology and Biological
807 Research Council project "Ricefuel" (grant numbers BB/K020358/1) awarded to H.J.G.
808 supported A.L. We thank Diamond Light Source for access to beamline I02, I04-1 and I24
809 (mx1960, mx7854 and mx9948) that contributed to the results presented here, and to Joes
810 Gray at Newcastle University for assistance with the mass spectrometry.

811

812 **Conflict of interest:** The authors declare that they have no conflicts of interest with the
813 contents of this article

814

815 **Author contributions**

816 Enzyme characterisation was carried out by A.S.L., J.B., X.Z., A.L., I.V. R.M., K.C., B.F., J.S.
817 The generation of oligosaccharide products by M-C.R., X.Z., A.S.L., A.C. and D.N. Gene
818 deletion strains were constructed by A.S.L., D.N., R.M., B.F., J.B. and D.W.A. Co-culturing
819 experiments were carried out by J.B. and A.S.L. Phylogenetic reconstruction and
820 metagenomic analysis was by N.T. and B.H. Bacterial growth and transcriptomic
821 experiments: Y.X., E.C.L. and E.C.M. X-ray protein crystallography was by A.B., A.C., A.S.L.
822 and J.B. N.M.R. experiments was by A.S.L. and K.S. Experiments were designed by D.W.A.,
823 H.J.G. and E.C.L., S.C.M. and H.J.G. The manuscript was written by H.J.G. with substantial
824 contributions from D.W.A. E.C.L., N.T. and B.H. Figures were prepared by E.C.L. and A.S.L.

825

826

827

828 **FIGURE LEGENDS**

829

830 **Figure 1. Genomic organization of pectin PULs.** **a**, Schematic of pectin structure
831 showing the different polysaccharides highlighted with different coloured
832 backgrounds. The respective linkages and monosaccharide composition are
833 represented according to the Symbol Nomenclature for Glycans system⁵⁰. **b**, genes
834 encoding proteins of known or predicted functionalities are colour coded. GHs, CEs
835 and PLs located in a known CAZy family are indicated by GHXX, CEXX or PLXX
836 where XX indicates the number of the family.

837

838 **Figure 2. Depolymerization of pectins at the cell surface of *B. thetaiotaomicron***
839 **cell surface.** **a**, Growth of wild-type and mutants of *B. thetaiotaomicron* (BtWT and
840 Δ btxxxx) or *B. ovatus* (BoWT and Δ bacovaxxxx) in minimal media containing the
841 indicated pectic polysaccharide; HG, homogalacturonan; SBA, sugar beet arabinan;
842 RGI-AM, rhamnogalacturonan I backbone from Arabidopsis mucilage (biological
843 replicates, n=3, error bars denote s.e.m). **b**, BtWT, BoWT and mutants lacking
844 functional outer membrane enzymes were incubated with appropriate
845 polysaccharides in aerobic conditions for the times indicated. Under these conditions
846 substrate is only available to the surface enzymes. Products released from the
847 glycans were monitored by High performance anion exchange chromatography
848 (HPAEC) with pulsed amperometric detection (PAD) or UV detection at 235 nm
849 (Abs_{235nm}). The degree of polymerisation of the peaks corresponding to the
850 galactose (Gal) and arabinose (Ara) oligosaccharides are shown in subscript
851 numbers. **c**, Western blot detection of selected *B. thetaiotaomicron* enzymes
852 encoded by the HG-PUL and RGI-PUL after treatment with proteinase K (PK+) or
853 untreated (-). BT4661 is a known surface glycan binding protein (control)⁶. The
854 cellular localization is indicated as periplasmic (P) or cell surface (CS). The example
855 is from biological replicates n=3. The full western blots are shown in **Supplementary**
856 **Fig. 1**.

857

858 **Figure 3. Signal molecule protection.** Each panel shows the affinities of the signal
859 molecules to respective sensors (top) and the catalytic efficiency of key enzymes
860 implicated in signal molecule degradation (bottom) for **a**, galactan, **b**, arabinan and **c**,
861 RGI. The data were from technical replicates, $n \geq 3$.

862 **Figure 4. Cross-feeding of polysaccharide breakdown products between**
863 ***Bacteroides* species.** **a**, Wild type *B. thetaiotaomicron* (WT) and mutants of the
864 bacterium lacking the key surface degrading enzymes for each polysaccharide were
865 mono-cultured and co-cultured with the wild type bacterium as indicated. Samples
866 were taken at different time points. The colony forming units of these samples were
867 determined by plating onto rich media (top panels) and the ratio of each bacterium in
868 the culture (bottom panel) was determine by qPCR with primers unique to each
869 strain. Error bars represent the s.e.m of biological replicates (n=3). **b**, *B. ovatus* (Bo),
870 *B. massiliensis* (Bm) and *B. uniformis* were mono-cultured or co-cultured with wild
871 type *B. thetaiotaomicron* (Bt) using the same experimental approach described in **a**.

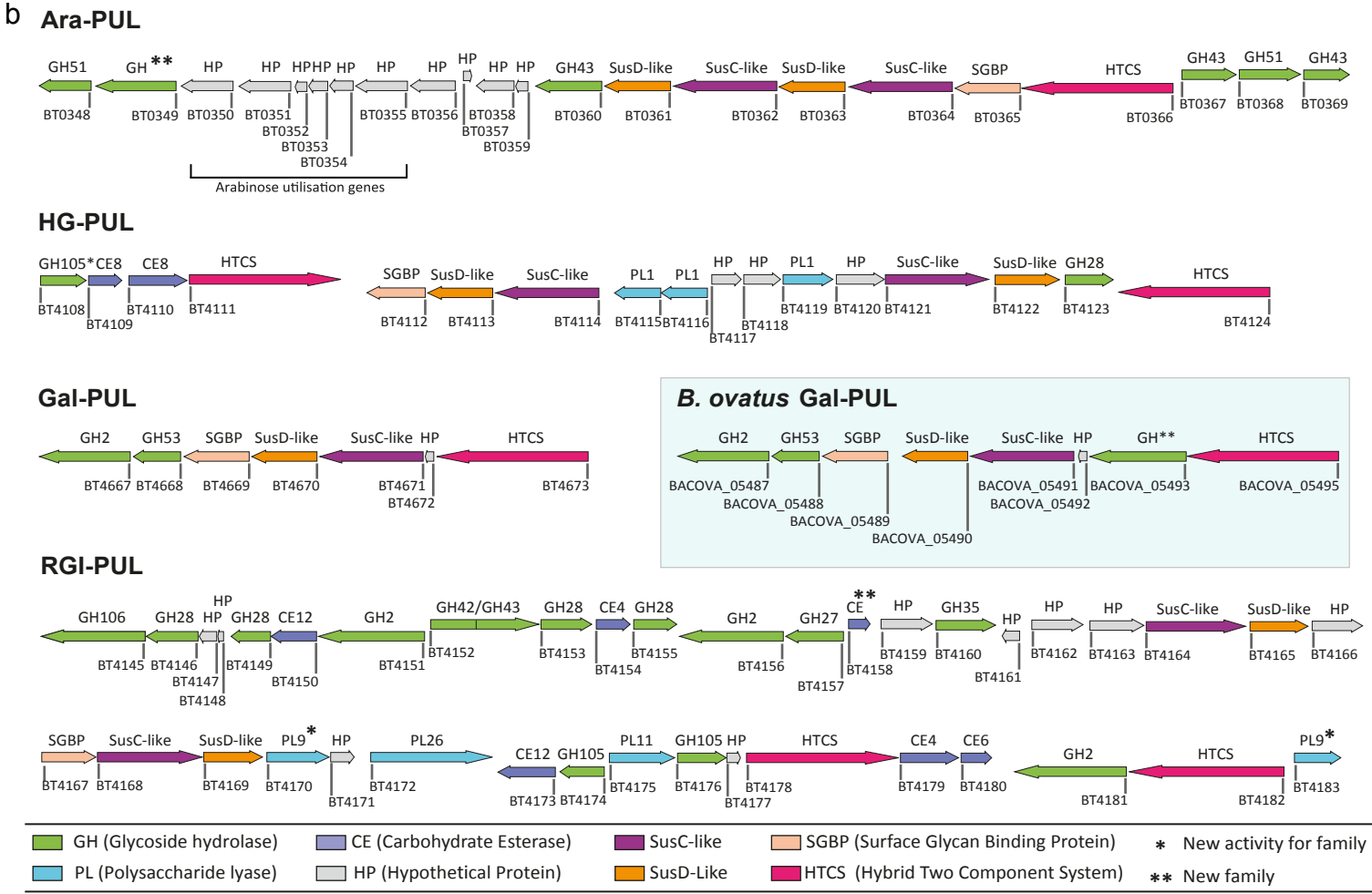
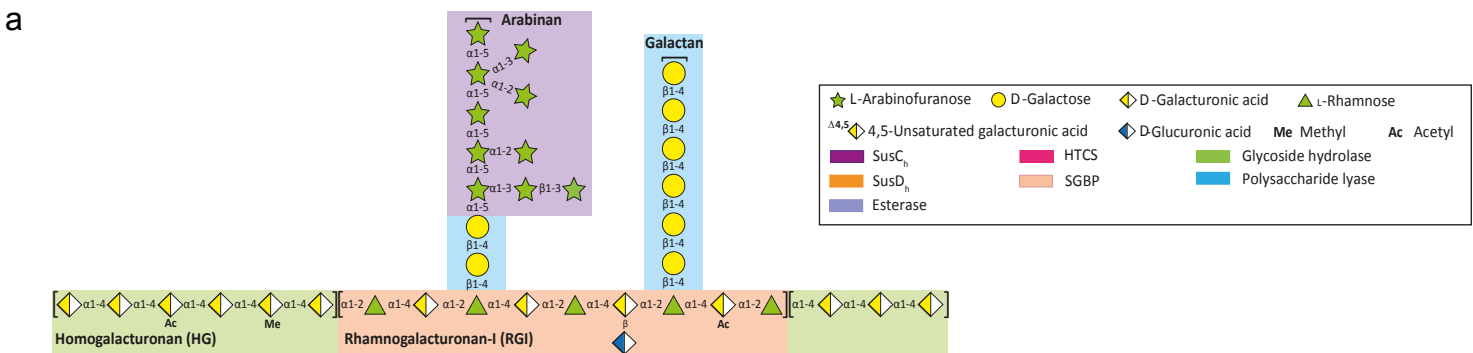
872

873

874

875

876 **Figure 5. Model of pectin utilization by *B. thetaiotaomicron*.** Chemical structures
877 of the sugars in the major pectins (a) Models for degradation of galactan (b, blue),
878 arabinan (c, purple), homogalacturonan (d, green) and rhamnogalacturonan I (e,
879 peach) are displayed. The black arrows indicate the linkage cleaved by the various
880 enzymes, while the grey arrows show the direction of the degradative pathway.
881



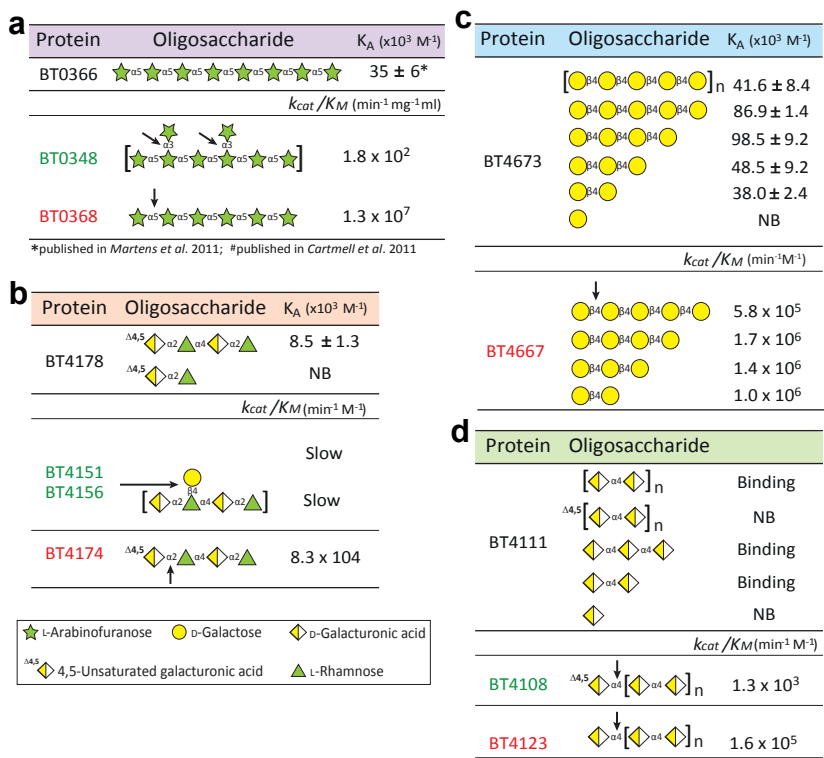


Figure 3. Signal molecule protection. Each panel shows the affinities of the signal molecules to respective sensors (top) and the catalytic efficiency of key enzymes implicated in signal molecule degradation (bottom) for **a**, galactan, **b**, arabinan, **c**, RGI and **d**, HG. The data were from technical replicates, $n \geq 3$.

FIGURE 3

